

Coherence properties of red blood cell membrane motions

Gabriel Popescu, YongKeun Park, Ramachandra R. Dasari, Kamran Badizadegan,* and Michael S. Feld
G. R. Harrison Spectroscopy Laboratory, Massachusetts Institute of Technology, Cambridge, Massachusetts 02139, USA
 (Received 28 December 2006; revised manuscript received 30 April 2007; published 7 September 2007)

We use a highly sensitive, noncontact, optical interferometric technique to quantify the red blood cell membrane fluctuations at the nanometer and millisecond scales. The results reveal significant properties of both temporal and spatial coherence associated with the membrane dynamics. We show that these correlations can be accounted for by the viscoelastic properties of the cell membrane. From this measurement, we extract the loss and storage moduli associated with the membrane and find a crossover frequency at which the buffer viscosity seems to become dominant.

DOI: [10.1103/PhysRevE.76.031902](https://doi.org/10.1103/PhysRevE.76.031902)

PACS number(s): 87.16.Dg, 87.15.Ya, 87.19.Tt

Red blood cell (RBC) membrane fluctuations have been studied intensively, as they offer a potential window into the structure, dynamics, and function of the cell [1–10]. In spite of these efforts, the molecular level interaction between the lipid bilayer and underlying cytoskeleton network and how it impacts on the overall mechanical properties of the cell is insufficiently known. Recently, it has been predicted that the 2D protein network that constitutes the RBC cytoskeleton confines the fluctuations of the bilayer, which has the net effect of an increased apparent superficial tension in the membrane [6]. We quantified experimentally this increase in tension by analyzing the time averaged (static) behavior of the RBC membrane displacements [9]. In contrast, very little is known about the dynamic behavior of RBCs. This information is relevant in the context of cell deformation during oxygen transport in the microvasculature and may provide insight into possible deterministic phenomena driven by active proteins [7,10]. In addition, understanding the dynamics of the RBCs bilayer-cytoskeleton complex has impact onto the general problem of membrane biophysics with broad applications to other cell types.

Optical techniques for investigating RBC motions can retrieve information without physical contact. However, this is a challenging task, as the membrane motions occur at the nanometer and millisecond scales. Existing methods, including phase contrast microscopy (PCM) [1], reflection interference contrast microscopy (RICM) [11], and fluorescence interference contrast (FLIC) [12] are limited in their ability to measure cell membrane displacements. PCM provides phase shifts quantitatively only for samples that are optically much thinner than the wavelength of light. Similarly, a single RICM measurement cannot provide the absolute cell thickness unless additional measurements or approximations are made [13]. FLIC relies on inferring the position of fluorescent dye molecules attached to the membrane from the absolute fluorescence intensity, which may limit both the sensitivity and acquisition rate of the technique [14].

In this paper, we use diffraction phase microscopy (DPM) [15,16], a quantitative phase imaging technique, to measure

the spatial and temporal coherence of RBC membrane motions. DPM relies on measuring the spatial interference fringes created by the superposition of a laser microscope image field and a uniform reference beam [Fig. 1(a)]. The quantitative phase image is obtained from a single recorded interferogram via a 2D Hilbert transform, which enables studying rapid phenomena [17]. The RBCs lay flat on a cover slip and are imaged in transmission through an immersion objective, in an inverted geometry. Thus the bottom leaflet of the cell membrane is fixed to the glass, while the top leaflet is freely fluctuating, which is the phenomenon of interest. The physical profile of the cell is obtained by using the homogeneous refractive index information that is specific to RBCs [18,19]. Due to its compact interferometric geometry, DPM is very stable, and thus sensitive to optical phase changes. For the 100 \times microscope objective used (oil immersion, numerical aperture NA=1.3), the transverse resolution was 200 nm and the overall optical path-length stability was 0.5 nm. This value is 2 times larger than obtained previously with the same instrument equipped with a 40 \times objective (no immersion) [16], which suggests that the immersion oil is responsible for this increase in the phase noise level. Throughout our experiments, we recorded series of RBC quantitative phase images for 4 s at a rate of 128 frames/s. Importantly, these DPM measurements do not require active stabilization, which is a significant advantage over our earlier measurements, where the static behavior of membrane flickering was studied [9].

We measured 15 live RBC cells of normal (discoid) shape, which were prepared for imaging according to a standard procedure [9]. Figure 1(c) shows the instantaneous membrane displacement map $\Delta h(x, y, t=0.5 \text{ s})$ of the RBC in Fig. 1(b). Approximating the membrane with a sheet of entropic springs, the equivalent elastic constant $k_e = 1.90 \pm 0.25 \mu\text{N/m}$ was measured, as described in Ref. [20], where the dynamics of RBC membranes is studied during morphological changes. The instantaneous restoring force, $f_e(x, y) = -k_e \Delta h(x, y)$, is shown in Fig. 1(d) to fall within $(-0.2, 0.2)$ pN. We calculated the autocorrelation function, $\langle \Delta h(t) \Delta h(t + \tau) \rangle$, at each point on the cell. Figure 1(e) shows this displacement autocorrelation for the three points indicated in Fig. 1(d). The FWHM (full width half maximum) of the autocorrelation function was used to map the entire projected area of the cell [Fig. 1(f)]. This temporal coherence

*Also at Department of Pathology, Harvard Medical School and Massachusetts General Hospital, Boston, Massachusetts 02114. gpopescu@mit.edu

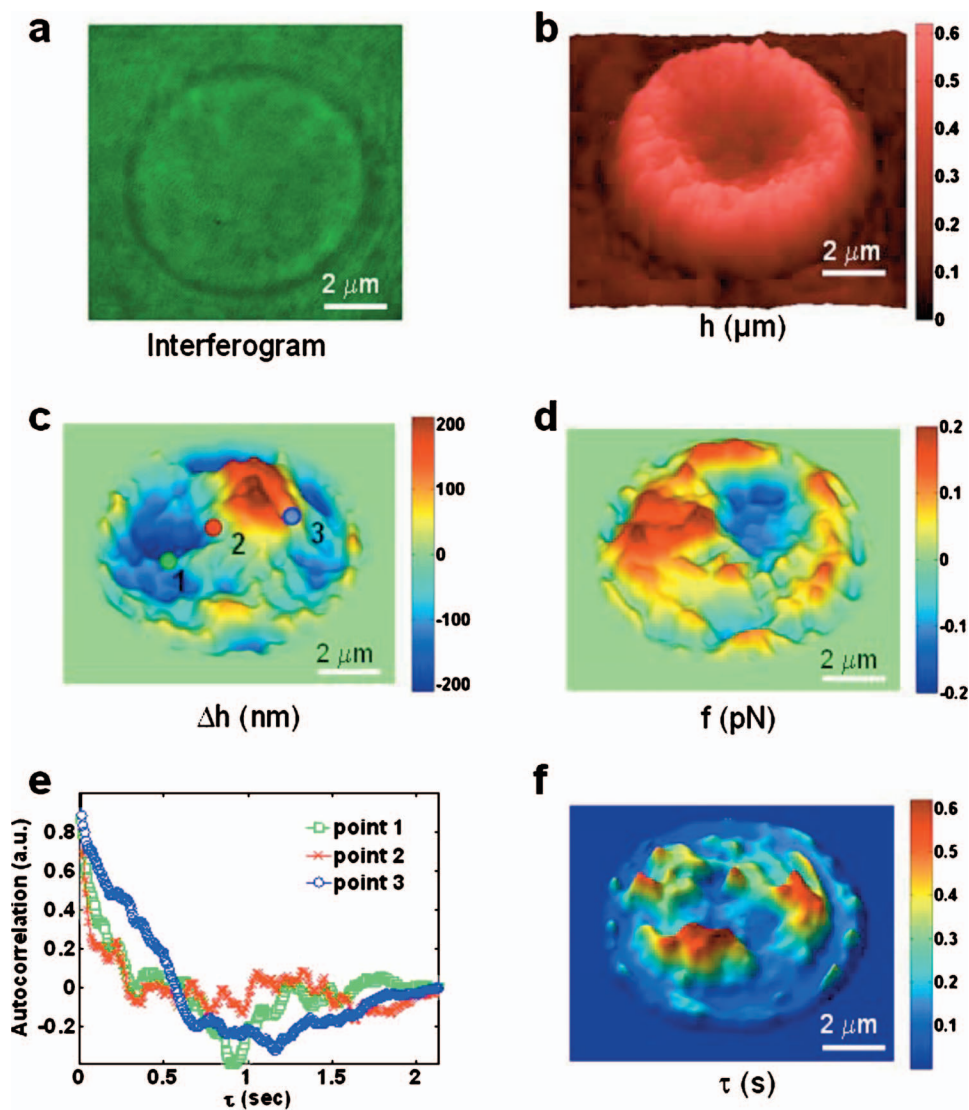


FIG. 1. (Color) DPM dynamic imaging of RBCs. (a) Interferogram of an RBC. (b) DPM image (physical map of the cell). (c) Instantaneous displacement map. (d) Instantaneous restoring force map. (e) Temporal autocorrelation of the displacements associated with the points shown in (c). (f) Map of the coherence times.

map is highly inhomogeneous and in some areas reaches values of up to 0.6 s.

In order to assess the spatial correlations associated with the membrane motions, we applied the formalism of coherence in the space-frequency domain developed by Mandel and Wolf for electromagnetic field fluctuations [21,22]. Thus, for each cell, we computed the *cross-spectral density*, $W(\mathbf{r}, \omega) = \int h^2(\mathbf{q}, \omega) e^{i\mathbf{q}\cdot\mathbf{r}} d^2\mathbf{q}$, which is a measure of the spatial correlations between two points separated by a distance $\rho = |\mathbf{r}|$ at a particular frequency ω [Fig. 2(a)]. This function W provides the full information about the spatiotemporal correlations of the membrane fluctuations. Using $W(\rho, \omega)$ as the weighting function, the transverse coherence length of the fluctuations, $\rho_c(\omega)$ can be computed for each individual frequency [Fig. 2(b)]. These long-range spatial correlations are affected by the cytoskeleton network. Therefore, quantifying the coherence area provides insight into the structural integrity of the protein (spectrin) mesh. Interestingly, the transverse coherence length shows a sharp increase below frequencies of ~ 2 Hz. This behavior at low frequencies appears to support the picture of ATP-mediated contributions at low frequencies reported in Ref. [2]. In addition, the saturation of

the coherence at the origin, i.e., $\rho_c(0) \approx 2 \mu\text{m}$, can be regarded as the effect of “fragmentation” in the membrane dynamic map observed in Fig. 1(f). Thus these coherence domains of about $1.5 \mu\text{m}$ in size localize the fluctuations and reduce the coherence area to lower values than in the case of a free membrane. Our previous measurements of membrane fluctuations over long time scales (minutes) revealed dominant frequencies which may also suggest deterministic motions [19]. These results are compatible with earlier measurements performed by Korenstein and co-workers [2,23]. However, independent studies of such effects are necessary before a definite conclusion can be drawn.

These coherence properties can be interpreted as the result of the viscoelastic properties of the cell membrane. Thus, assuming the model of a continuous elastic sheet under the action of both surface tension and bending, the membrane equation of motion can be written as [10]

$$\dot{h}(\mathbf{q}, t) + \omega(\mathbf{q})h(\mathbf{q}, t) = \Lambda(\mathbf{q})f(\mathbf{q}, t), \quad (1)$$

where h is the height of the element of membrane, \mathbf{q} the spatial wave vector, $\omega(\mathbf{q}) = (\kappa\mathbf{q}^3 + \sigma\mathbf{q})/4\eta$, κ the bending

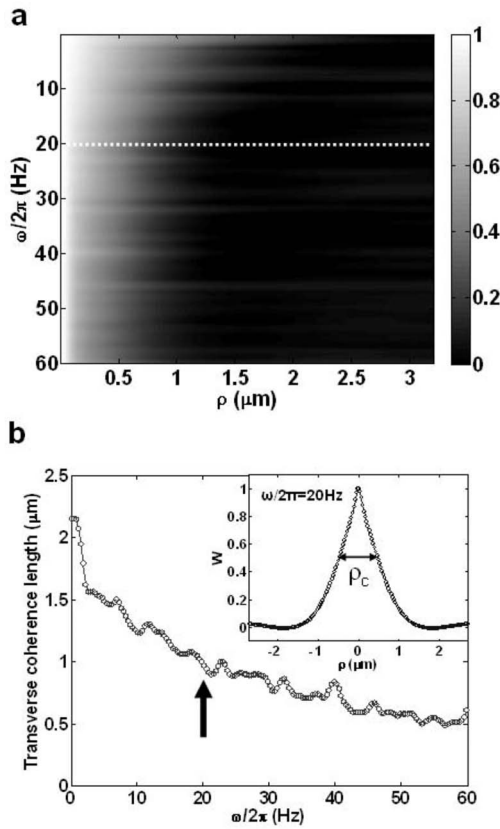


FIG. 2. (a) The cross spectral density of the cell shown in Fig. 1. (b) Transverse coherence length ρ_c vs frequency. The inset shows the profile of W along the dash line in (a) and shows how ρ_c is defined.

modulus, σ the tension modulus, η the viscosity of the surrounding medium, f the random force, and $\Lambda(q) = 1/(4\eta q)$ is the Oseen tensor. It can be shown that the solution for height autocorrelation function can be expressed in the general form as

$$\langle h(\mathbf{q}, t)h(\mathbf{q}, t + \tau) \rangle = \frac{\Lambda^2(\mathbf{q})}{\omega(\mathbf{q})} e^{-\omega(\mathbf{q})\tau} \otimes \langle f(\mathbf{q}, t)f(\mathbf{q}, t + \tau) \rangle. \quad (2)$$

In Eq. (2), \otimes denotes the temporal convolution operation and the angular brackets indicate temporal averaging. At thermal equilibrium, $\langle f(\mathbf{q}, t)f(\mathbf{q}, t + \tau) \rangle = 2k_B T \delta(\tau) / \Lambda(\mathbf{q})$, which defines the lack of temporal correlation in the force fluctuations. However, the elasticity of the membrane provides the motions with “memory,” which results in a coherence time of the order of $1/\omega(q)$. Therefore, under the conditions of thermodynamic equilibrium, by exploiting the fluctuation-dissipation theorem (FDT) and the generalized Stokes-Einstein relationship (GSER), the storage and loss moduli can be extracted from the fluctuation measurement. This approach has been used in the past for passive microrheology probed by embedded colloidal particles [24,25].

A typical measured nanoscale fluctuation power spectrum in both temporal frequency and spatial frequency domain, $|\Delta h(q, \omega)|^2$, is shown in Fig. 3(a). The dissipative component

(imaginary part) of the membrane response function is inferred from the fluctuation-dissipation theorem,

$$\chi''(\mathbf{q}, \omega) = \frac{\pi\omega}{k_B T} \Delta h(\mathbf{q}, \omega)^2, \quad (3)$$

where T is the absolute temperature and k_B is Boltzmann's constant [Fig. 3(b)]. The storage component (real part) of the response function is obtained using the Kramers-Kronig relationship, which connects the real and imaginary parts of χ and reflects the causality of the system [Fig. 3(c)]. We used the GSER to retrieve the complex viscoelastic modulus

$$G(\mathbf{q}, \omega) = \frac{1}{6\pi\Lambda} \frac{1}{\chi(\mathbf{q}, \omega)}, \quad (4)$$

where $\Lambda = 2\pi/q$ is the spatial wavelength of the membrane fluctuations. Note that the unit of $G(q, \omega)$ is Pa/m^2 . The loss (viscous) modulus G'' is obtained as the imaginary part of G [Fig. 3(d)], and the storage (elastic) modulus G' is the real part of G [Fig. 3(e)]. The spatially averaged complex modulus $G(\omega)$ is obtained by applying the FD theorem as

$$G(\omega) = \frac{1}{6\pi} \int \frac{1}{2\pi q \Lambda \chi(q, \omega)} dq. \quad (5)$$

The unit of $G(\omega)$ is Pa, which is commonly used in rheology.

The results in terms of G' and G'' for the group of 15 RBCs are summarized in Fig. 3(f). The frequency behavior is similar to that obtained in polymer solutions, which is not surprising, given that the spectrin network of the membrane cytoskeleton is responsible for the overall shear resistance of the cell membrane [25]. Over the frequency range 5–50 Hz, the storage and dissipation moduli approach power law behaviors, $G' \propto \omega^{0.58 \pm 0.08}$ and $G'' \propto \omega^{0.71 \pm 0.1}$, where the errors indicate the cell to cell variations ($N=15$). It is well known that $G'' \propto \omega^1$ describes a Newtonian fluid, while $G'' \propto \omega^0$ indicates a solid behavior. Thus the intermediate exponent of 0.71 simply states that the membrane is a viscoelastic fluid. A power spectrum dependence $\Delta h^2(\omega) \propto \omega^{-5/3}$ has been predicted for free membranes [26] and further used to describe experimental data on artificial polymerized membranes [27]. Using Eqs. (3) and (4), it can be easily seen that their results would give $G'' \propto \omega^{0.66}$, which agrees very well with what we measured. In our previous measurements (Ref [9].), we found an exponent of -1.54 for discocytes in the low- q regime, which falls between this $-5/3$ value, but is also compatible with the $-4/3$ exponent reported by others [1,6]. For RBCs transitioning to the echinocyte and spherocyte, the G'' exponent decreases consistently, which indicates stronger confinement of the membrane motions [28]. There is a particular frequency, $\omega/2\pi = 35$ Hz, above which the viscous modulus becomes dominant, i.e., the cell transitions towards a dissipation-dominated regime, which is most likely due to the buffer viscosity.

Compared to current techniques of assessing cell viscoelasticity such as pipette aspiration [29], electric field deformation [30], optical tweezers [31], and magnetic bead excitation [32], our DPM method has the distinct advantage of

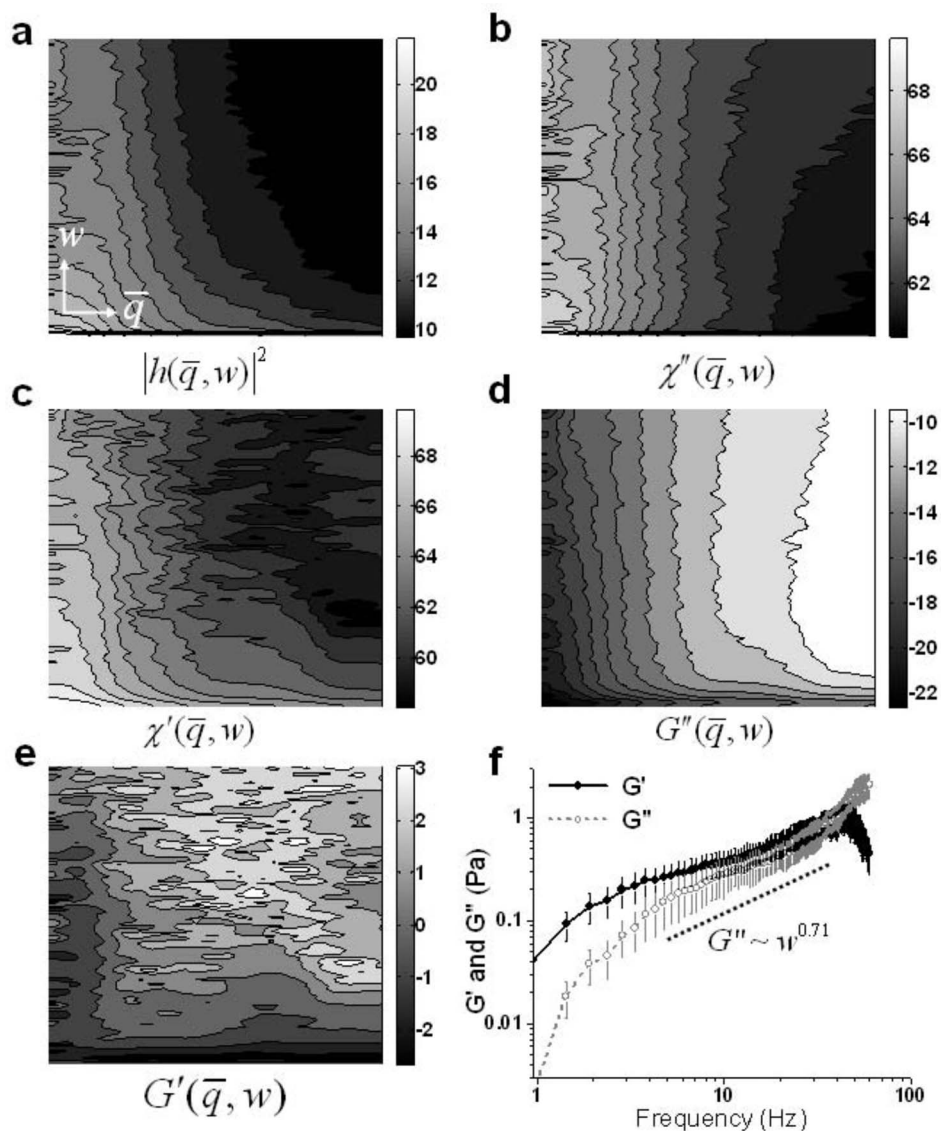


FIG. 3. Retrieving the viscoelastic moduli from the DPM data. (a) Power spectrum of displacement vs spatial and temporal frequencies. (b) Imaginary part of the response function. (c) Real part of the response function. (d) Dissipation modulus. (e) Storage modulus. (f) Spatially averaged viscous (G'') and elastic (G') moduli. The error bars correspond to cell-to-cell variations ($N=15$).

being noncontact. Further, our measurements offer, for the first time to our knowledge, the spatiotemporal complex response function $\chi(\mathbf{q}, \omega)$ of the viscoelastic membrane. The complex modulus $G(\omega)$ captures the dynamic behavior of the system and is analogous to the shear modulus that has been measured in 3D complex fluids. While the derivation of G in Pa corresponds to a shear modulus, its interpretation has to

be made with care, as the Hamiltonian describing the fluctuations contains bending and tension terms. Thus G represents an *effective* complex modulus that describes the global dynamics of the membrane at thermal equilibrium. Current experiments in our laboratory are directed towards comparing this approach to the results provided by particle membrane excitation.

[1] F. Brochard and J. F. Lennon, *J. Phys. (France)* **36**, 1035 (1975).
 [2] S. Levin and R. Korenstein, *Biophys. J.* **60**, 733 (1991).
 [3] D. H. Boal, U. Seifert, and A. Zilker, *Phys. Rev. Lett.* **69**, 3405 (1992).
 [4] S. Tuvia, S. Levin, and R. Korenstein, *FEBS Lett.* **304**, 32 (1992).
 [5] S. Tuvia, A. Almagor, A. Bitler, S. Levin, R. Korenstein, and S. Yedgar, *Proc. Natl. Acad. Sci. U.S.A.* **94**, 5045 (1997).

[6] N. Gov, A. G. Zilman, and S. Safran, *Phys. Rev. Lett.* **90**, 228101 (2003).
 [7] N. Gov, *Phys. Rev. Lett.* **93**, 268104 (2004).
 [8] L. C. L. Lin and F. L. H. Brown, *Phys. Rev. Lett.* **93**, 256001 (2004).
 [9] G. Popescu, T. Ikeda, K. Goda, C. A. Best-Popescu, M. Laposata, S. Manley, R. R. Dasari, K. Badizadegan, and M. S. Feld, *Phys. Rev. Lett.* **97**, 218101 (2006).
 [10] L. C. L. Lin, N. Gov, and F. L. H. Brown, *J. Chem. Phys.* **124**,

- 074903 (2006).
- [11] A. Zilker, H. Engelhardt, and E. Sackmann, *J. Phys. (France)* **48**, 2139 (1987).
- [12] A. Lambacher and P. Fromherz, *J. Opt. Soc. Am. B* **19**, 1435 (2002).
- [13] A. Zidovska and E. Sackmann, *Phys. Rev. Lett.* **96**, 048103 (2006).
- [14] Y. Kaizuka and J. T. Groves, *Phys. Rev. Lett.* **96**, 118101 (2006).
- [15] G. Popescu, T. Ikeda, R. R. Dasari, and M. S. Feld, *Opt. Lett.* **31**, 775 (2006).
- [16] Y. K. Park, G. Popescu, K. Badizadegan, R. R. Dasari, and M. S. Feld, *Opt. Express* **14**, 8263 (2006).
- [17] T. Ikeda, G. Popescu, R. R. Dasari, and M. S. Feld, *Opt. Lett.* **30**, 1165 (2005).
- [18] G. Popescu, T. Ikeda, C. A. Best, K. Badizadegan, R. R. Dasari, and M. S. Feld, *J. Biomed. Opt. Lett.* **10**, 060503 (2005).
- [19] G. Popescu, K. Badizadegan, R. R. Dasari, and M. S. Feld, *J. Biomed. Opt. Lett.* **11**, 040503 (2006).
- [20] Y. K. Park, C. A. Best-Popescu, K. Badizadegan, R. R. Dasari, M. S. Feld, and G. Popescu (unpublished).
- [21] L. Mandel and E. Wolf, *Rev. Mod. Phys.* **37**, 231 (1965).
- [22] L. Mandel and E. Wolf, *Optical Coherence and Quantum Optics* (Cambridge University Press, Cambridge, UK, 1995).
- [23] S. Tuvia, S. Levin, A. Bitler, and R. Korenstein, *J. Cell Biol.* **141**, 1551 (1998).
- [24] T. G. Mason and D. A. Weitz, *Phys. Rev. Lett.* **74**, 1250 (1995).
- [25] G. Popescu, A. Dogariu, and R. Rajagopalan, *Phys. Rev. E* **65**, 041504 (2002).
- [26] A. G. Zilman and R. Granek, *Phys. Rev. Lett.* **77**, 4788 (1996).
- [27] E. Helfer, S. Harlepp, L. Bourdieu, J. Robert, F. C. MacKintosh, and D. Chatenay, *Phys. Rev. Lett.* **85**, 457 (2000).
- [28] Y. K. Park, C. A. Best-Popescu, K. Badizadegan, R. R. Dasari, M. S. Feld, and G. Popescu (unpublished).
- [29] D. E. Discher, N. Mohandas, and E. A. Evans, *Science* **266**, 1032–5 (1994).
- [30] H. Engelhardt, H. Gaub, and E. Sackmann, *Nature (London)* **307**, 378 (1984).
- [31] M. Dao, C. T. Lim, and S. Suresh, *J. Mech. Phys. Solids* **51**, 2259 (2003).
- [32] L. H. Deng, X. Trepate, J. P. Butler, E. Millet, K. G. Morgan, D. A. Weitz, and J. J. Fredberg, *Nat. Mater.* **5**, 636 (2006).